Mitochondrial Defects in the Respiratory Complex I Contribute to Impaired Translational Initiation via ROS and Energy Homeostasis in SMA Motor Neurons

Maximilian Paul Thelen
Institute of Human Genetics, University of Cologne, 50931, Cologne, Germany 2Center for Molecular Medicine, Cologne, University of Cologne, 50931, Cologne, Germany

Brunhilde Wirth
Institute of Human Genetics, University of Cologne, 50931, Cologne, Germany 2Center for Molecular Medicine, Cologne, University of Cologne, 50931, Cologne, Germany

Min Jeong Kye (Min.kye@uk-koeln.de)
Institute of Human Genetics, University of Cologne, 50931, Cologne, Germany 2Center for Molecular Medicine, Cologne, University of Cologne, 50931, Cologne, Germany

Research article

Keywords: Spinal muscular atrophy, SMN, mitochondria, reactive oxygen species, translation initiation

Posted Date: August 14th, 2020

DOI: https://doi.org/10.21203/rs.3.rs-49251/v1

Abstract

Background

Spinal muscular atrophy (SMA) is a neuromuscular disease, characterized by loss of lower alpha motor neurons, which leads to proximal muscle weakness. SMA is caused by reduced levels of Survival of Motor Neuron (SMN) due to biallelic deletions or mutations in the *SMN1* gene and mainly non-functional *SMN2* copy gene. When SMN levels fall under a certain threshold, a plethora of cellular pathways are disturbed including RNA processing, protein synthesis, metabolic defects and dysfunctional mitochondria. Dysfunctional mitochondria can harm cells by decreased ATP production, but also by increased oxidative stress due to elevated production of reactive oxygen species (ROS). Since neurons mainly produce energy via mitochondrial oxidative phosphorylation to cover their high energy demands, restoring metabolic/ oxidative homeostasis can be beneficial in SMA pathology.

Methods

We performed whole proteome analysis of murine primary motor neurons using mass spectrometry to identify molecular mechanisms altered by SMN deficiency, which contribute to SMA pathology. Identified pathways were independently confirmed by biochemical and molecular biological methods as well as imaging analysis. Furthermore, cellular energy and ROS levels were biochemically measured in WT and SMA motor neurons.

Results

We report that primary SMA motor neurons show disturbed energy homeostasis such as a reduced number of functional mitochondria, impaired glucose uptake and overall lower basal ATP concentrations. In addition, elevated ROS levels cause an increase of protein carbonylation and impaired protein synthesis efficiency in SMA motor neurons. Counteracting these cellular impairments with supplemented pyruvate reduced elevated ROS levels, increased ATP and SMN protein levels in SMA motor neurons. Furthermore, we found that pyruvate-mediated SMN protein synthesis is mTOR-dependent. Most importantly, we show that ROS regulates global protein synthesis at the translational initiation step, which is impaired in SMA.

Conclusion

In summary, we found that excessive amount of cellular ROS caused by defective mitochondria inhibits initiation of mRNA translation, which results in pathological phenotypes often observed in degenerative neurons. As many neuropathies share patho-phenotypes such as dysfunctional mitochondria, excessive ROS and impaired protein synthesis.Our findings suggest a new molecular networking system among these pathways.

Background

Spinal muscular atrophy is an inherited neuromuscular disease that is characterized by the loss of lower motor neurons (MNs) due to dramatically reduced levels of the ubiquitously abundant Survival of Motor Neuron (SMN) protein [1]. The incidence of SMA varies between 1 per 6000–10000 newborns [2]. In 94% of individuals with SMA homozygous deletions or gene conversion of *SMN1*, that encodes only full length SMN protein, have been described [2]. Instead the number of the almost identical *SMN2* copy gene that mainly produces a transcript lacking exon 7 due to a single silent mutation in exon 7 [3], inversely correlates with disease severity [4]. *SMN2* encodes for a rapidly degraded, unstable SMN protein, which is destroyed by the proteasome pathway [5, 6]. SMN forms a stable complex with other proteins called Gemin2-8 [7]. It is still not clear how the loss of a ubiquitously expressed protein like SMN leads to cell type specific degeneration in lower alpha MNs. SMN is an RNA binding protein that performs multiple essential cellular functions including biogenesis of small nuclear ribonucleoproteins (snRNPs) [8] and trafficking of mRNAs to axon terminals [9–11]. Furthermore, SMA cells show dysregulated splicing and miRNA processing [12, 13], hyperexcitability and impaired Ca^{2+} homeostasis [14–16], reduced protein synthesis efficiency [10, 17, 18] and impaired axon growth [11].

Recent evidence suggests that energy metabolism is impaired in SMA [19–21]. Within mitochondrial energy production by the oxidative phosphorylation (OXPHOS), the NADH: ubiquinone oxidoreductase (complex I) of the electron transport chain is the rate limiting step in respiration and the major entry point for electrons [22]. Complex I is also the major producer of reactive oxygen species (ROS) in mitochondria [23]. Therefore, dysfunctional complex I can impair energy production as well as ROS homeostasis. ROS can function as signaling molecules by activating different pathways including the MAPK, PI3K, Akt, p38 MAPK and Ca^{2+} signaling [22], but also harm cells by irreversible oxidative protein modifications such as carbonylation [24, 25]. In particular to SMN, oxidative stress can hinder the SMN complex formation [26].

The mammalian target of rapamycin complex 1 (mTORC1) acts as an integral node between cellular energy production and consumption. It promotes anabolic processes but also restricts catabolic processes such as autophagy [27–29]. Anabolic processes promoted by mTORC1 include mitochondrial biogenesis [30] and protein synthesis [31]. The protein synthesis is a coupled process of translation initiation and elongation. Especially cap-dependent translation initiation is promoted by mTORC1. The rate limiting step in translation initiation is the association of the cap-binding protein, eukaryotic translation initiation factor 4E (eIF4E) into the eIF4F complex, that recruits the small ribosomal unit to mRNAs [32]. Translation initiation is repressed by the eukaryotic initiation factor 4E (eIF4E)-binding protein 1 (4E-BP1) [33]. mTORC1 phosphorylates 4E-BP1 and promotes the dissociation of 4E-BP1 from eIF4E to increase cap-dependent translation [34]. Furthermore, translation initiation is promoted by phosphorylation of S6 kinase (S6K), phosphorylating eIF4B. Besides translational initiation, mTOR promotes ribosomal biogenesis through phosphorylation of the ribosomal protein S6, downstream of the S6K.

In low doses, ROS can stimulate mTOR activity, but in high doses, oxidative stress decreases it [35, 36]. Previous research has indicated that phosphorylation of 4E-BP1, 4E-BP2 and the ribosomal protein S6 is

abolished by mTOR inhibition [37]. It is also known that mTOR regulates translation of a subset of mitochondria- related mRNAs [37].

Here, we first report the molecular mechanism explaining how mitochondria regulate protein synthesis via ATP and ROS production in MNs. Furthermore, when this pathway is disturbed, it contributes to pathology of the MN disorder, SMA. Particularly, cellular ATP and ROS signaling regulates protein synthesis efficiency at the translational initiation step. Our finding implies that mitochondria control neuronal energy and ROS homeostasis as well as protein synthesis via mTOR pathway.

Materials And Methods

Animal model

The 'Taiwanese' SMA mouse model (on FVB background) carrying two *SMN2* copies on one allele on a murine *Smn* null background [38], was established by breeding $Smn^{KO/KO}$; $SMN2^{tg/tg}$ mice with $Smn^{KO/WT}$ mice (Hsieh-Li et al. 2000) resulting in 50% SMA mice ($Smn^{KO/KO}$; $SMN2^{tg/0}$) and 50% phenotypically normal heterozygous littermates ($Smn^{KO/WT}$; $SMN2^{tg/0}$) [39].

Primary Motor Neuron Culture

E13.5 embryos were used for primary spinal MN culture. SMA embryos were genotyped as previously described [39] using the KAPA mouse genotyping kit (Sigma) before further processing. Spinal cords were isolated and dissociated with 1% trypsin (Worthington) in PBS. Single cell suspension was achieved by trituration with DNase I (Applichem) in plating medium (DMEM supplemented with 5% fetal calf serum (Biochrom), 0.6% glucose, penicillin/streptomycin (Thermo Fisher Scientific) and amphotericin B (Promocell). For imaging analyses, 15,000 cells/cm^2 were plated on poly-D-lysine (PDL, 10 µg/ml, Sigma) coated coverslips, and for biochemical analyses 120,000 cells/cm^2 were plated on PDL coated cell culture plates with neuronal plating media. Neuronal plating media was replaced the following day, by MN maintenance medium (Neurobasal medium with B27 supplement (Thermo Fisher Scientific), 2 mM L-glutamine, penicillin/streptomycin and amphotericin B with additional growth factors: brain derived neurotrophic factor (BDNF, 10 ng/ml, PeproTech), ciliary neurotrophic factor (CNTF, 10 ng/ml, PeproTech), and glia cell line derived neurotrophic factor (GDNF, 10 ng/ml, PeproTech). Half of the medium was exchanged every third day, and cytosine arabinoside (AraC) was added after 3 days to a final concentration of 1 µM. Cells were cultured at 37 °C in a humidified incubator with 5% CO_2.

Culture Of Cell Lines

Motor neuron-like NSC-34 cells were cultured in Dulbecco's Modified Eagle's Medium (DMEM) with 10% fetal calf serum, 1% penicillin/streptomycin and amphotericin B. 20,000 cells/cm^2 were plated in PDL

coated 12- well plates. Differentiation was induced by 50 µM retinoic acid (Sigma) for 3 days. Cells were maintained at 37 °C in a humidified incubator with 5% CO_2.

Rna Isolation, Cdna Synthesis And Real-time Pcr

Total RNA was extracted from cells using the mirVana™ miRNA Isolation Kit (Thermo Fisher Scientific) according to manufacturer's instructions. cDNA was produced from total RNA using the High-Capacity cDNA Reverse Transcription Kit (Thermo Fisher Scientific) with random primers. mRNA expression levels were quantified with PowerSYBR® Green PCR Master Mix (Thermo Fisher Scientific) and 1 µM of gene specific primers using real-time PCR (7500 Real-Time PCR System, Thermo Fisher Scientific). Specificity of the primers was confirmed by Sanger's sequencing. Sequences of primers are listed in Supplementary table 1.

Protein Isolation And Western Blot Analysis

Proteins were extracted with RIPA buffer (Sigma) supplemented with protease and phosphatase inhibitors (Thermo Fisher Scientific) and protein concentration was determined by Pierce™ BCA protein assay kit (Thermo Fisher Scientific). Western blot analysis was performed with standard protocol. The information about antibodies are listed in Supplementary table 2. Signals were detected with ChemiDoc XRS + System (BioRad) using ECL chemiluminescence (Thermo Scientific), and signals were quantified by using the ImageLab 6.0 software (BioRad).

Drug Treatment

Primary motor neurons and NSC34 cells were supplemented in culture with the following substances at given concentrations in each figure: The supplements sodium pyruvate and sodium lactate, the anti-oxidant N-acetylcysteine (NAC), the ROS inducer menadione, the protein synthesis inhibitor anisomycin (all purchased from Sigma) and the water soluble mTOR inhibitor WYE-687 dihydrochloride (Tocris) (Supplementary table 4).

Proteomics Of Primary Motor Neurons

Primary MNs were treated with 50 mM pyruvate (Sigma), 10 µM N-acetylcystein (NAC, Sigma) and 100 µM Menadione (Sigma) for 1 hour, lysed in RIPA buffer (Sigma) with protease and phosphatase inhibitors and further processed for mass spectrometry (MS) analysis. Proteins were precipitated using ice-cold acetone at -80 °C for 15 min and at -20 °C for 2 hours. Pellets were resuspended in 8 M urea buffer with protease inhibitor. This was followed by an in-solution reduction using 5 mM dithiothreitol (DTT) at room temperature (RT) for 1 h, an alkylation with 40 mM chloroacetamide (CAA) in the dark for 30 min, and digestion with endo-proteinase Lys-C for 4 hours at RT. Samples were diluted with 50 mM

Triethylammoniumbicarbonate (TEAB) to a final concentration of Urea ≤ 2 M following digestion with trypsin over night at RT. To stop enzymatic digestion, samples were acidified with 1% formic acid. Acidified samples were purified with styrenedivinylbenzene-reverse phase sulfonate (SDB-RPS) Stage Tips. Proteomic analysis was performed with ultra-high-performance liquid chromatography (UHPLC) coupled to a Quadrupole-Orbitrap mass spectrometer (Thermo Fisher Scientific) (CECAD/ CMMC Proteomics core facility, University of Cologne). Raw data were analyzed by MaxQuant. As reference, a canonical mouse database from Uniprot (22.08.19) was used. For gene ontology (GO) analysis, the Database for Annotation, Visualization and Integrated Discovery 6.7 (DAVID) was used. Statistical analysis and data visualization were performed using RStudio. We used the mouse MitoCarta 2.0 dataset to identify mitochondrial proteins [40]. Additional data about identified proteins and GO analysis are listed in Additional file 3 MS Source data.

Sunset Assay (surface Sensing Of Translation)

Protein synthesis was measured by SUnSET assay [41]. Tyrosyl-tRNA analogue, puromycin labelled newly synthesized proteins during protein elongation. Prior puromycin labelling, cells were treated with ROS modifying drugs or 50 µM anisomycin (Sigma) as a negative control. Afterwards, cells were incubated with 1 µM of puromycin (Thermo Fisher Scientific) for 30 min. Finally, puromycin labelled peptides were detected by western blotting or immunostaining using an anti-puromycin antibody.

Sunrise (sunset-based Ribosome Speed Of Elongation)

The SunRiSE assay was used to monitor protein elongation speed [42]. Initiation of mRNA translation was blocked by 2 µg/ml harringtonine (Abcam) at different time points, and all samples were incubated with 10 µg/ml (16.7 µM) puromycin for 10 min. Puromycin labelled peptides were detected by western blotting.

Mitotracker® And Immunostaining Of Mns

Cells were incubated with MitoTracker® Red CMXRos (Thermo Fisher Scientific) at a final concentration of 100 nM for 15 min and fixed with paraformaldehyde (PFA) [13]. The information about antibodies can be found in Supplementary Table 3. Images were acquired with a fluorescence microscope (Zeiss Axio Imager.M2) equipped with an AxioCam MR camera and an ApoTome.2 system (Institute of Human Genetics, University of Cologne). Images were analyzed with FIJI. All image analyses were performed blindly.

Atp Assay

Intracellular ATP concentrations were measured with ATP determination kit (Thermo Fisher Scientific) based on bioluminescence signal detection by GloMax® luminescence reader (Promega, Institute of Human Genetics, University of Cologne). ATP levels were normalized to the amount of soluble proteins determined by BCA assay.

Glucose Uptake Assay

Glucose Uptake-Glo kit (Promega) was used to measure glucose uptake efficiency using 120,000 cells/cm^2 cells. We mainly followed the manufacturer's instruction and luminescence was detected by the GloMax luminescence reader (Promega). Signal was normalized to protein concentration measured by BCA assay.

Pyruvate Uptake Assay

Pyruvate uptake was measured with Pyruvate assay kit (Sigma). Fluorescence signal was measured with the Safire 2 microplate reader (Tecan) and normalized to soluble protein amount.

Detection Of Oxidative Stress

CellROX™ Green reagent (Thermo Fisher Scientific) was used to measure oxidative stress. To compare the oxidative stress level between WT and SMA MNs, cells were incubated with 5 µM CellROX™ Green reagent for 30 min. After fixation with 3.7% formaldehyde, nuclei and F-actin were labelled with DAPI and Alexa Fluor™ 568 Phalloidin (Thermo Fisher Scientific) respectively. Images were acquired with a fluorescence microscope equipped with an ApoTome.2 system. CellROX™ signal was quantified with Safire 2 microplate reader (Tecan). Signals of the microplate reader were normalized to soluble protein concentration after lysis with RIPA buffer (Sigma). To monitor oxidative stress after manipulation of ROS levels in cells, 50 mM pyruvate, 10 µM NAC, and 100 µM Menadione were added 45 min before measure. Signal was quantified with the Safire 2 microplate reader (Tecan).

Protein Carbonylation Assay

The amount of protein carbonyl groups created by oxidation was measured with the Protein carbonyl assay kit (Abcam). Proteins were quantified by Bradford.

Aha-click It Assay

L-azidohomoalanine (AHA, Thermo Fisher Scientific) is incorporated into proteins during active protein synthesis and later on detected by click chemistry reaction with biotin alkyne. To deplete endogenous

methionine reserves, cells were incubated with HBSS for 30 min. For AHA labelling, 500 μM L-AHA with/without drugs were treated for 1 hour. After incubation at 37 °C, cells were washed and lysed with RIPA buffer with protease and phosphatase inhibitors on ice. Click chemistry reaction was achieved with Click-iT® protein reaction buffer kit (Thermo Fisher Scientific). We followed manufacturer's protocol.

Statistical analysis

Statistical analysis was conducted in R version 3.6.2 using RStudio [43]. All graphs for cell biology experiments are presented as mean ± s.d. For normally distributed variables, statistical significance was analyzed with t-test (two-tailed). Multiple comparisons are corrected with the Holm-Bonferroni method. Differences among group means are determined with Tukey's honestly significant difference (HSD) test after rejection of the null hypothesis by one-way analysis of variance (ANOVA). Normally distributed experimental results with two factors are analyzed by two-way ANOVA with Tukey HSD post-hoc analysis. To compare multiple mean values to a single control mean in time course and dose-response experiments Dunnett's post hoc test was used after one-way ANOVA. Statistical tests were applied only to biological replicates, even when data is presented as individual measurement counts. Significance is indicated by stars (*$p < 0.05$; **$p < 0.01$; *** <0.001, n.s. = not significant).

Results

Mitochondria are defective in SMA MNs, resulting in an impaired energy homeostasis

To investigate differentially expressed proteins and discover dysregulated pathways in SMA, we used primary MNs isolated from an SMA mouse model and wild-type mice [38]. Whole proteome analysis of 10 days *in vitro* (DIV) MNs detected 5165 proteins of which 681 (~ 13%) are mitochondria related (Fig. 1a and Fig. S1a, b). Among all identified proteins, 494 proteins were significantly changed in SMA compared to WT, and 61 (~ 12%) of them are localized to mitochondria based on MitoCarta2.0 database (Fig. 1a, b). Among these 61 proteins, 11 proteins are localized to the oxidative phosphorylation (OXPHOS) machinery (Fig. S1c). Interestingly, in the OXPHOS machinery, complex I seems mainly affected in SMA with 9 dysregulated proteins (Fig. S1c). To understand the biological meaning of SMA affected proteins, we analyzed gene ontology (GO) terms of all 345 significantly down-regulated and 149 significantly up-regulated proteins (Fig. 1c, d). Among the down-regulated proteins in SMA MNs we identified previously documented pathways in SMA pathology such as RNA binding, protein transport, ribonucleoprotein complexes and protein synthesis confirming the reliability of the data set (Fig. 1c) [8–11, 17]. 149 up-regulated proteins suggested mitochondrial dysfunction in ATP production (Fig. 1d). Therefore, we further investigated localization and function of mitochondria in motor axons using MitoTracker and TOM20 (Fig. 1e). Indeed, numbers of total and functional mitochondria are reduced in SMA axons (Fig. 1e). The finding of mitochondrial mis-localization is strengthened by down-regulated mitochondrial motor proteins KIF5B and KIF5BP in SMA MNs in our whole proteome analysis using mass spectrometry (MS) (Fig.

S1b). In addition, mitochondria are smaller and fragmented in SMA MNs (Fig. S1d). As neurons can produce energy from glycolysis to compensate for their high energy demand [44], glucose uptake was monitored. Interestingly, glucose uptake is also impaired in SMA MNs (Fig. 1f). As both energy producing pathways are impaired in SMA MNs, we next measured the intracellular ATP concentrations. Indeed, ATP concentration is up to 3-fold lower in SMA compared to WT MNs (Fig. 1g). Together, these results suggest that energy homeostasis is impaired in SMA MNs due to defective mitochondria and glycolysis is unable to compensate for this defect.

Proteins are hyper-carbonylated and protein synthesis is impaired in SMA

As our MS results indicated defects in complex I of the electron transport chain and complex I is known source of reactive oxygen species (ROS) in mitochondria [23], we measured intracellular ROS levels using CellROX® (Fig. 2a, b). Indeed, our data indicated that ROS levels were increased in SMA compared to WT (Fig. 2a). This finding was confirmed by two independent detection methods; imaging and microplate reader (Fig. 2a and b). In heathy condition, ROS can be eliminated by oxidative stress defense proteins such as superoxide dismutase (SOD1), which clears ROS from the mitochondrial intermembrane space [45]. Interestingly, SOD1 protein levels are down-regulated in SMA MNs, indicating defective oxidative stress defense mechanism in SMA (Fig. S1b). As oxidative stress results in carbonylation of proteins [46], we measured levels of carbonylated proteins in SMA MNs (Fig. 2c). Indeed, higher amounts of carbonylated proteins were detected. This data confirmed our finding that SMA MNs are under oxidative stress (Fig. 2c). Carbonylation of proteins can alter their conformation and hinder their protein synthesis [24, 47]. Furthermore, as levels of ribosomes and translation related proteins are also changed in SMA due to our MS data, we measured protein synthesis efficiency with Surface sensing of translation (SUnSET) and AHA-Click it assay in WT and SMA MNs (Fig. 2d-g). Indeed, we confirmed that SMA MNs show a reduced protein synthesis efficiency compared to WT with two independent methods (Fig. 2d-g). Taken together, these results suggest a negative correlation between ROS levels and protein synthesis.

Pyruvate restores ATP levels and reduces ROS levels in SMA

Next, we pursued to restore the consequence of defective mitochondria in SMA; energy deficiency and oxidative stress. As pyruvate is known to reduce ROS in a non-enzymatic way and is a known substrate of TCA cycle [48], we supplemented WT and SMA MNs with 10 mM or 50 mM sodium pyruvate. Within 1 hour of treatment with 50 mM pyruvate, ATP levels were increased significantly in MN-like NSC-34 cells (Fig. S2c) and SMA MNs (Fig. 3a and Fig. S2f), while no effect was seen in WT MNs (Fig. 3a and Fig. S2f). However, lactate, which can be converted to pyruvate by lactate dehydrogenase in the cytoplasm [49], neither altered ATP levels in NSC-34 cell (Fig. S2d, e) nor in primary MNs (Fig. S2f). In addition, as pyruvate has been suggested as a ROS scavenger [50], we treated SMA MNs with pyruvate and measured ROS levels. Indeed, pyruvate could successfully reduce ROS levels in SMA MNs (Fig. 2b). Further, we confirmed pyruvate uptake and ROS reduction by treatment with 50 mM pyruvate or 10 µM of the anti-oxidant NAC in ROS induced cells by menadione treatment (Fig. S2a, g). These results suggest that

pyruvate is a valuable supplement to restore ATP levels and simultaneously balance intracellular ROS levels in MNs.

Effect Of Ros On Protein Synthesis In Neurons

Based on our data, we hypothesized that the elevated ROS levels hinder protein synthesis, thus, reduction of ROS might restore impaired protein synthesis in SMA MNs. In order to further understand the effect of ROS on protein synthesis, we have modified cellular ROS levels in MNs and measure protein synthesis efficiency. We treated MNs with 10 μM NAC or 50 mM pyruvate or 100 μM menadione and performed SunSET analysis (Fig. 4a). Protein synthesis efficiency was unaltered by pyruvate or NAC in WT MNs (Fig. 4b). However, menadione-induced ROS clearly inhibited protein synthesis. As a positive control, 50 μM anisomycin was used (Fig. 4b-d). The same results were observed in NSC-34 cells (Fig. S3a-c). Interestingly, for SMA MNs, where cellular ROS levels are higher, a reduction of ROS by adding 10 μM NAC could increase protein synthesis (Fig. 4c). However, no consistent increase of protein synthesis was observed in pyruvate supplemented SMA MNs (Fig. 4c). In addition, SunSET signal was visualized and quantified by immunofluorescent staining in MNs. Indeed, these results confirmed that NAC can restore impaired protein synthesis in SMA MNs (Fig. 4d). Taken together, modulation of ROS has an effect on protein synthesis in MNs.

Whole Proteome Analysis Of Mns With Ros Manipulation

Next, we tried to obtain a systemic view of the whole proteome regulated by ROS in MNs. First, cells were incubated with 50 mM pyruvate for 1 hour, and whole proteome was analyzed by MS. We found that the levels of 122 proteins were altered in SMA MNs (Fig. 5a, c). Gene ontology (GO) analysis of altered proteins revealed proteins related to ATP production, which were enriched in all three terms (Fig. 5b). The biological process of oxidative phosphorylation was enriched, and the cellular compartment of mitochondria was affected by pyruvate supplement (Fig. 5b). In addition, ribonucleotide binding, spliceosome, RNA splicing, and mRNA processing were also affected by pyruvate. Interestingly, these terms have been reported as altered pathways in SMA (Fig. 5b). Among 122 proteins, 22 were also significantly changed by pyruvate in WT MNs, and 28 were significantly altered in pyruvate treated SMA MNs (Fig. 5c-e). Interestingly, when we compare proteins altered in SMA to pyruvate affected proteins in WT or SMA MNs, we found that the effect of pyruvate was clearer in SMA MNs (Fig. 5d, e). Next, we compared the levels of proteins altered by pyruvate in an isolated view. Among those 28 proteins, 21 proteins were down-regulated in SMA and up-regulated by pyruvate. GO analysis of these 21 proteins revealed a strong enrichment in ATP binding and mRNA processing (Fig. 5f). In contrast, pyruvate changed levels of 144 proteins in WT MNs, and among them 22 proteins were also altered in SMA compared to WT (Fig. S4a-f). However, these 22 proteins showed far less changes after pyruvate treatment (Fig. S5a, e). Due to the small changes in WT MNs, only few GO terms were identified (Fig. S4c).

Next, SMA MNs were treated with 10 μM NAC, a known antioxidant, for 1 hour. Whole proteome analysis showed that 143 proteins were significantly changed (Fig. 5g, i). GO analysis suggested these proteins have multiple functions including nucleotide binding and RNA processing (Fig. 5h). Compared with differentially expressed proteins between WT and SMA MNs, 31 proteins were common with NAC treatment in SMA MNs (Fig. 5i). Among them, 17 proteins were down-regulated in SMA compared to WT, and up-regulated by NAC treatment (Fig. 5k, l). Interestingly, these proteins also regulate RNA processing and splicing (Fig. 5l). Again, NAC showed only little effect on individual proteins in WT MNs (Fig. 5j), while it showed clear effect on SMA MNs (Fig. 5j, k, and Fig. S4g-l). ROS induction by 100 μM menadione for 1 h in WT MNs had the biggest effects on the proteome with 344 significantly altered proteins (Fig. S4m, o). In addition, menadione induced ROS also showed the biggest overlap of altered proteins with SMA affected proteins; 56 proteins (Fig. S4n-p). GO analysis revealed strong enrichment in nucleotide-binding and association with mitochondria (Fig. S4r). It is worthy to mention that pyruvate and NAC had only a small effect on WT MNs, whereas they can induce a large up-regulation of proteins in SMA MNs. This could be because basal amounts of these proteins were lower in SMA MNs compared to WT MNs.

Ros Regulates Initiation Of Mrna Translation

Due to GO analysis, a major biological process, mRNA translation is dysregulated in SMA MNs. The volcano plot illustrates 360 proteins found in our MS data related to mRNA translation based on the MGI database (Fig. 6a). Among them, 40 out of 47 are significantly down-regulated in SMA MNs compared to WT ones (Fig. 6a). mRNA translation is tightly regulated in eukaryotic cells by two major processes; initiation and elongation. As we already know that efficiency of protein synthesis is impaired in SMA MNs [9, 10, 17], we deciphered further mechanisms to determine which step is disrupted by SMN loss. To distinguish between the effects of initiation and elongation, we measured both processes in MNs. First, to assess the rate of protein elongation, we used the SunRiSE assay. In brief, translation initiation was blocked by 2 μg/ml harringtonine at different time intervals, before newly synthesized peptides were tagged with 10 μg/ml puromycin (Fig. 6b). Puromycin tagged proteins were detected by Western blot with anti-puromycin antibody. Data analysis did not show any clear changes in the elongation rate in neither WT nor SMA MNs after supplementation of NAC or pyruvate (Fig. 6c, d).

As translational elongation is unaltered by SMA or ROS, we next focused on translational initiation. One of the well described translational initiation mechanisms is cap-dependent translation initiation by 4E-BP1 (eukaryotic translation initiation factor 4E-binding protein 1). Therefore, we measured the phosphorylation status of 4E-BP1 after modulation of ROS levels. Reduced phosphorylation status of 4E-BP1 indicates that initiation of mRNA translation is indeed impaired in SMA MNs (Fig. 6e). No significant difference was observed by pyruvate or NAC in WT cells (Fig. 6f). While induction of ROS by 100 μM menadione resulted in a reduction of 4E-BP1 phosphorylation, suggesting excessive ROS can inhibit mRNA translation at the initiation step (Fig. 6f). Furthermore, pyruvate and NAC increased the phosphorylation of 4E-BP1 in SMA MNs (Fig. 6g). Taken together, this unprecedented data reveals that

mRNA translation is impaired at the initiation step in SMA MNs, while elongation is unaltered. Moreover, initiation of mRNA translation is regulated by ROS via 4E-BP1.

SMN protein levels are regulated by pyruvate and ROS via mTOR

Most interestingly, pyruvate supplement did not only increase ATP levels and reduce ROS, but also increased SMN levels in WT and SMA MNs as well as NSC-34 cells (Fig. 7a, b, and Fig. S5a, e). To understand the molecular mechanism underlying increased SMN levels, we measured *Smn* mRNA levels in WT MNs and NSC-34 cells after pyruvate treatment (Fig. S5b). No significant increase of *Smn* mRNA levels were observed, suggesting post transcriptional regulation of SMN levels (Fig. S5b). Next, protein synthesis inhibitor, anisomycin prevented the pyruvate induced increase of SMN protein levels (Fig. S5c). This data confirms that protein synthesis of SMN is regulated by pyruvate. In addition, 10 μM NAC increased SMN levels in MNs (Fig. 7c, d and Fig. S5e). As mTOR, especially mTORC1 is a major regulator of protein synthesis [51], we tested whether increase of SMN protein levels is mTOR dependent. We treated MNs with water-soluble mTOR blocker, 100 nM WYE-687 dihydrochloride and supplied 50 mM pyruvate. Indeed, pyruvate increased SMN levels in WT MNs and this effect was abolished by WYE-687 dihydrochloride (Fig. 7e). In addition, pyruvate increased mTORC1 activity measured by phosphorylation status of the S6K as well as its target ribosomal S6 protein (S6) in WT MNs (Fig. 7f, g and Fig. S5d). Further, reduction of ROS by NAC treatment in SMA MNs increased the mTORC1 activity (Fig. 7h). Taken together, our data showed that cellular ROS and ATP levels regulate SMN protein synthesis via regulating mTORC1. Furthermore, re-balancing ROS levels with anti-oxidant in SMA MNs can increase SMN protein synthesis.

Discussion

From a whole proteome analysis of SMA compared to WT MNs, we revealed that SMA MNs suffer from mitochondrial dysfunctions. Prior studies have noted the mitochondrial dysfunction in SMA MNs including decreased respiration, increased oxidative stress and impaired mitochondrial mobility [19, 21]. Here, we further investigated molecular mechanisms underlying mitochondrial dysfunction and found that the intracellular ATP concentration is lower and especially proteins of complex I of the electron transport chain in mitochondria were highly dysregulated in SMA MNs. These results provide further support for our hypothesis that impaired protein synthesis in SMA MNs is due to increased oxidative stress, as the majority of ROS is produced by mitochondrial complex I. While a previous report did not observe changes in the numbers of axonal mitochondria [21], we found a reduced number of axonal mitochondria. This controversary might be explained by methodological differences. In the previous study, mitochondria were labeled by aberrantly expressed mitochondrial proteins, while we used MitoTracker®, a membrane potential dependent dye, which does not stain non-functional mitochondria or antibodies against the mitochondrial protein TOM20. This implicates that proportion of dysfunctional mitochondria in SMA axon is higher compared to WT ones.

While neurons mainly use mitochondria as their energy sources, it has been suggested that they can obtain energy form glycolysis in energy demanding conditions [52]. Our results revealed that glucose uptake is impaired in SMA MNs, thus, reduced energy production by defective mitochondria is not compensated by glycolysis. Taken together, we could conclude that SMA MNs are under energy deprivation status due to mitochondrial defects as well as impaired glucose uptake. Glycolysis is impaired in other neurodegenerative diseases such as Alzheimer's disease (AD) and amyotrophic lateral sclerosis (ALS) [53, 54]. Furthermore, it has been proposed that enhancing glycolysis is neuroprotective in ALS [55]. However, it is not clear whether glycolysis is also impaired in SMA MNs.

As excessive cellular ROS are harmful to the cellular system, production and scavenging mechanisms are tightly regulated in all living organisms. Dysbalanced ROS has been reported in numerous pathological conditions [56, 57]. ROS can be produced by mitochondria and cleared up by enzymes and chelating agents [58]. With the current data, we can speculate that ROS production can be increased by defective mitochondria, but it is not clear whether ROS scavenging mechanisms are also altered in SMA MNs. Interestingly, we revealed that ROS regulates mRNA translation at the initiation step in MNs, and this mechanism is dysregulated in SMA MNs. Importantly, counteracting this molecular pathway by supplementation of pyruvate or anti-oxidant NAC shows restored impaired translational initiation in SMA MNs. Nevertheless, in WT MNs, reducing ROS had no effect on protein synthesis as WT MNs do not suffer from oxidative stress. This data intensifies our conclusion that healthy cells tightly regulate the balance of ROS levels, but SMN deficient cells lost their balance in ROS production and/or scavenging due to defective mitochondria. Furthermore, our data revealed that ROS regulates mRNA translation at the initiation step and this contributes to known SMA pathology, impaired protein synthesis.

Interestingly, reduction of ROS via pyruvate or anti-oxidant NAC lead to an increase of SMN protein levels mTOR dependently. An increase of SMN by pyruvate or NAC was also observed in WT MNs, even though it did not change overall protein synthesis rate. While the molecular mechanism is still unclear, out data suggest that pyruvate and NAC specifically increase SMN protein levels via mTOR without altering the whole proteome, and independent of oxidative stress. It has been reported that SMN is involved in ribosome biology and mTOR activity is reduced in SMA neurons [17, 18]. These findings suggest a SMN-specific feedback mechanism of gene expression. However, the clear mechanism underlying mTOR dependent SMN protein synthesis needs to be further identified. It has been unclear whether mRNA translation has mRNA-specific mechanisms, like transcription of genes can be selectively regulated by promoters and transcription factors. Our data strongly implies that a protein specific mRNA translation mechanism may exist in motor neurons.

Overall, we unraveled the previously unknown molecular connections between mitochondria and protein synthesis in neurons, and their dysfunction contributes to pathology of SMA, a genetic neuromuscular disorder via ROS.

Conclusion

This study describes a previously unknown mechanism, how defective mitochondria influence the pathology of SMA, especially impaired protein synthesis. With proteomics approach using an SMA mouse model, we found that mitochondria are defective. Especially proteins in the mitochondrial respiratory complex I are dysregulated in SMA MNs. Due to this, ATP levels are decreased, and ROS levels are increased. Furthermore, we were able to restore/rebalance the ATP and ROS levels in SMA motor neurons by supplementation of pyruvate. Modifying ROS levels influences protein synthesis at the translation initiation step, which is impaired in SMA motor neurons. In addition, pyruvate enhances SMN protein synthesis mTOR-dependently. As mitochondrial defects have been reported in other neurological disorders, our study reveals the basic cellular mechanism of how mitochondria can influence efficiency of protein synthesis in motor neurons. This study will lead to new insights into druggable pathways for neurological disorders, including SMA.

List Of Abbreviations

4E-BP1 eukaryotic initiation factor 4E (eIF4E)-binding protein 1

AD Alzheimer's disease

ALS amyotrophic lateral sclerosis

ATP adenosine triphosphate

Complex I NADH: ubiquinone oxidoreductase

DIV Days *in vitro*

eIF4E eukaryotic translation initiation factor 4E

GO gene ontology

MN motor neuron

mRN messenger ribonucleic acid

miRNA micro ribonucleic acid

mTORC1 mammalian target of rapamycin complex 1

NAC N-acetylcysteine

OXPHOS oxidative phosphorylation

RNA ribonucleic acid

ROS reactive oxygen species

S6 ribosomal protein S6

S6K S6 kinase

SDB-RPS styrenedivinylbenzene-reverse phase sulfonate

SMA Spinal muscular atrophy

SMN Survival of motor neuron

SOD1 Superoxide dismutase

SunRiSE SUnSET-based Ribosome Speed of Elongation

SUnSET Surface sensing of translation

TCA Tricarboxylic acid

WT wildtype

Declarations

Ethics approval

All animal breedings and procedures were performed in accordance with the institutional animal care guidelines and the German animal welfare laws. They are approved under the reference numbers 84-02.04.2015.A378 and UniKoeln_Anziege§4.16.020 of the LANUV (LandesamtfürNatur, Umwelt und Verbraucherschutz NRW) state agency of North-Rhine-Westphalia. FVB/N wild type mice were used as controls (Jackson).

Consent of publication

Not applicable.

Availability of data and materials

The mass spectrometry proteomics data have been deposited to the ProteomeXchange Consortium via the PRIDE [59] partner repository with the dataset identifierPXD020403

The results of the mass spectrometry dataset, supporting the conclusions of this article is included within the article as Additional file3: Mass Spectrometrysource data.

Competing interests

The authors declare that they have no conflict of interest.

Funding

This work is funded by SMA Europe Research grant to MK and Deutsche Forschungsgemeinschaft (DFG) KY96/1-2 to MK, and DFG Wi945/17-1, Research Training Group (RTG) 1960 to BW and Center for Molecular Medicine Cologne (CMMC) C16 to BW.

Authors' contributions

All authors contributed to the study conception and design. Material preparation, data collection and analysis were performed byMPT and MJK. The first draft of the manuscript was written by MPT and all authors commented on previous versions of the manuscript. All authors read and approved the final manuscript.

Acknowledgements

We are very grateful for the support of the proteomics and animal facility at the CECAD and CMMC of the University of Cologne.

References

1. Lefebvre S, Bürglen L, Reboullet S, Clermont O, Burlet P, Viollet L, et al. Identification and characterization of a spinal muscular atrophy-determining gene. Cell [Internet]. 1995;80:155–65. Available from: http://www.ncbi.nlm.nih.gov/pubmed/7813012.
2. 10.1146/annurev-genom-102319-103602
   Wirth B, Karakaya M, Kye MJ, Mendoza-Ferreira N. Twenty-Five Years of Spinal Muscular Atrophy Research: From Phenotype to Genotype to Therapy, and What Comes Next. Annual Review of Genomics and Human Genetics [Internet]. 2020;21:annurev-genom-102319-103602. Available from: https://www.annualreviews.org/doi/10.1146/annurev-genom-102319-103602.
3. 10.1073/pnas.96.11.6307
   Lorson CL, Hahnen E, Androphy EJ, Wirth B. A single nucleotide in the SMN gene regulates splicing and is responsible for spinal muscular atrophy. Proceedings of the National Academy of Sciences [Internet]. 1999;96:6307–11. Available from: http://www.pnas.org/cgi/doi/10.1073/pnas.96.11.6307.
4. Feldkötter M, Schwarzer V, Wirth R, Wienker TF, Wirth B. Quantitative analyses of SMN1 and SMN2 based on real-time lightcycler PCR: Fast and highly reliable carrier testing and prediction of severity of spinal muscular atrophy. Am J Hum Genet. 2002;70:358–68.
5. Chang HC, Hung WC, Chuang YJ, Jong YJ. Degradation of survival motor neuron (SMN) protein is mediated via the ubiquitin/proteasome pathway. Neurochem Int. 2004;45:1107–12.
6. Lorson CL, Strasswimmer J, Yao J-M, Baleja JD, Hahnen E, Wirth B, et al. SMN oligomerization defect correlates with spinal muscular atrophy severity. Nature Genetics [Internet]. 1998;19:63–6. Available from: http://www.nature.com/articles/ng0598-63.

7. Gubitz A. The SMN complex. Experimental Cell Research [Internet]. 2004;296:51–6. Available from: https://linkinghub.elsevier.com/retrieve/pii/S0014482704001338.
8. Pellizzoni L, Yong J, Dreyfuss G. Essential role for the SMN complex in the specificity of snRNP assembly. Science. 2002;298:1775–9.
9. Akten B, Kye MJ, Hao LT, Wertz MH, Singh S, Nie D, et al. Interaction of survival of motor neuron (SMN) and HuD proteins with mRNA cpg15 rescues motor neuron axonal deficits. Proc Natl Acad Sci USA. 2011;108:10337–42.
10. 10.1523/JNEUROSCI.3631-10.2011
Fallini C, Zhang H, Su Y, Silani V, Singer RH, Rossoll W, et al. The Survival of Motor Neuron (SMN) Protein Interacts with the mRNA-Binding Protein HuD and Regulates Localization of Poly(A) mRNA in Primary Motor Neuron Axons. Journal of Neuroscience [Internet]. 2011;31:3914–25. Available from: http://www.jneurosci.org/cgi/doi/10.1523/JNEUROSCI.3631-10.2011.
11. Rossoll W, Jablonka S, Andreassi C, Kröning AK, Karle K, Monani UR, et al. Smn, the spinal muscular atrophy-determining gene product, modulates axon growth and localization of β-actin mRNA in growth cones of motoneurons. J Cell Biol. 2003;163:801–12.
12. https://dx.plos.10.1371/journal.pone.0163954
Custer SK, Gilson TD, Li H, Todd AG, Astroski JW, Lin H, et al Altered mRNA Splicing in SMN-Depleted Motor Neuron-Like Cells. Singh RN, editor. PLOS ONE [Internet]. 2016;11:e0163954. Available from: https://dx.plos.org/10.1371/journal.pone.0163954.
13. Gonçalves IDCG, Brecht J, Thelen MP, Rehorst WA, Peters M, Lee HJ, et al. Neuronal activity regulates DROSHA via autophagy in spinal muscular atrophy. Scientific Reports. Nature Publishing Group; 2018;8.
14. Jablonka S, Beck M, Lechner BD, Mayer C, Sendtner M. Defective Ca2 + channel clustering in axon terminals disturbs excitability in motoneurons in spinal muscular atrophy. Journal of Cell Biology [Internet]. 2007;179:139–49. Available from: https://rupress.org/jcb/article/179/1/139/34887/Defective-Ca2-channel-clustering-in-axon-terminals.
15. Morita M, Gravel S-P, Chénard V, Sikström K, Zheng L, Alain T, et al. mTORC1 Controls Mitochondrial Activity and Biogenesis through 4E-BP-Dependent Translational Regulation. Cell Metabolism [Internet]. Nature Publishing Group; 2013;18:698–711. Available from: http://www.nature.com/srep/2015/150720/srep12189/full/srep12189.html.
16. 10.1016/j.neuron.2010.12.032
Mentis GZ, Blivis D, Liu W, Drobac E, Crowder ME, Kong L, et al. Early Functional Impairment of Sensory-Motor Connectivity in a Mouse Model of Spinal Muscular Atrophy. Neuron [Internet]. Elsevier Inc.; 2011;69:453–67. Available from: http://dx.doi.org/10.1016/j.neuron.2010.12.032.
17. 10.1093/hmg/ddu350
Kye MJ, Niederst ED, Wertz MH, Gonçalves I do Akten CG, Dover B KZ, et al. SMN regulates axonal local translation via miR-183/mTOR pathway. Human Molecular Genetics [Internet]. 2014;23:6318–

31. Available from: https://academic.oup.com/hmg/article-lookup/doi/10.1093/hmg/ddu350.

18. Bernabò P, Tebaldi T, Groen EJN, Lane FM, Perenthaler E, Mattedi F, et al. In Vivo Translatome Profiling in Spinal Muscular Atrophy Reveals a Role for SMN Protein in Ribosome Biology. Cell Reports. Elsevier BV. 2017;21:953–65.

19. 10.1002/jnr.22106/full
Acsadi G, Lee I, Li X, Khaidakov M, Pecinova A, Parker GC, et al. Mitochondrial dysfunction in a neural cell model of spinal muscular atrophy. Journal of Neuroscience Research [Internet]. 2009;87:2748–56. Available from: http://onlinelibrary.wiley.com/doi/10.1002/jnr.22106/full.

20. http://dx.plos.10.1371/journal.pgen.1006744
Boyd PJ, Tu W-Y, Shorrock HK, Groen EJN, Carter RN, Powis RA, et al Bioenergetic status modulates motor neuron vulnerability and pathogenesis in a zebrafish model of spinal muscular atrophy. Cox GA, editor. PLOS Genetics [Internet]. 2017;13:e1006744. Available from: http://dx.plos.org/10.1371/journal.pgen.1006744.

21. Miller N, Shi H, Zelikovich AS, Ma Y-C. Motor neuron mitochondrial dysfunction in spinal muscular atrophy. Human Molecular Genetics [Internet]. 2016;25:3395–406. Available from: http://www.ncbi.nlm.nih.gov/pubmed/27488123.

22. Sharma L, Lu J, Bai Y. Mitochondrial Respiratory Complex I. Structure, Function and Implication in Human Diseases. Curr Med Chem. 2009;16:1266–77.

23. Liu Y, Fiskum G, Schubert D. Generation of reactive oxygen species by the mitochondrial electron transport chain. Journal of neurochemistry [Internet]. 2002;80:780–7. Available from: http://www.ncbi.nlm.nih.gov/pubmed/11948241.

24. Stadtman ER. Metal ion-catalyzed oxidation of proteins: Biochemical mechanism and biological consequences. Free Radic Biol Med. 1990;9:315–25.

25. 10.1038/s41467-017-02694-8
Topf U, Suppanz I, Samluk L, Wrobel L, Böser A, Sakowska P, et al. Quantitative proteomics identifies redox switches for global translation modulation by mitochondrially produced reactive oxygen species. Nature Communications [Internet]. Springer US; 2018;9:324. Available from: http://dx.doi.org/10.1038/s41467-017-02694-8.

26. Wan L, Ottinger E, Cho S, Dreyfuss G. Inactivation of the SMN complex by oxidative stress. Molecular cell [Internet]. 2008;31:244–54. Available from: https://linkinghub.elsevier.com/retrieve/pii/S1097276508003936.

27. Hara T, Mizushima N. Role of ULK-FIP200 complex in mammalian autophagy: FIP200, a counterpart of yeast Atg. 17? Autophagy. 2009;5:85–7.

28. Noda T, Ohsumi Y. Tor, a phosphatidylinositol kinase homologue, controls autophagy in yeast. J Biol Chem. 1998;273:3963–6.

29. Scott RC, Schuldiner O, Neufeld TP. Role and regulation of starvation-induced autophagy in the Drosophila fat body. Dev Cell. 2004;7:167–78.

30. Cunningham JT, Rodgers JT, Arlow DH, Vazquez F, Mootha VK, Puigserver P. mTOR controls mitochondrial oxidative function through a YY1-PGC-1α transcriptional complex. Nature. 2007;450:736–40.
31. 10.1101/gad.887201
Gingras AC, Raught B, Sonenberg N. Regulation of translation initiation by FRAP/mTOR. Genes & development [Internet]. 2001;15:807–26. Available from: http://www.genesdev.org/cgi/doi/10.1101/gad.887201.
32. 10.1016/j.molcel.2012.04.004
Yanagiya A, Suyama E, Adachi H, Svitkin Y, v., Aza-Blanc P, Imataka H, et al. Translational Homeostasis via the mRNA Cap-Binding Protein, eIF4E. Molecular Cell [Internet]. Elsevier Inc.; 2012;46:847–58. Available from: http://dx.doi.org/10.1016/j.molcel.2012.04.004.
33. Pause A, Belsham GJ, Gingras A-C, Donzé O, Lin T-A, Lawrence JC, et al. Insulin-dependent stimulation of protein synthesis by phosphorylation of a regulator of 5'-cap function. Nature [Internet]. 1994;371:762–7. Available from: http://www.nature.com/articles/371762a0.
34. 10.1101/gad.13.11.1422
Gingras A-C, Gygi SP, Raught B, Polakiewicz RD, Abraham RT, Hoekstra MF, et al. Regulation of 4E-BP1 phosphorylation: a novel two-step mechanism. Genes & Development [Internet]. 1999;13:1422–37. Available from: http://www.genesdev.org/cgi/doi/10.1101/gad.13.11.1422.
35. 10.1016/j.cellsig.2010.05.015
Li M, Zhao L, Liu J, Liu A, Jia C, Ma D, et al. Multi-mechanisms are involved in reactive oxygen species regulation of mTORC1 signaling. Cellular Signalling [Internet]. Elsevier Inc.; 2010;22:1469–76. Available from: http://dx.doi.org/10.1016/j.cellsig.2010.05.015.
36. 10.1242/jcs.226258
Topf U, Uszczynska-Ratajczak B, Chacinska A. Mitochondrial stress-dependent regulation of cellular protein synthesis. Journal of Cell Science [Internet]. 2019;132:jcs226258. Available from: http://jcs.biologists.org/lookup/doi/10.1242/jcs.226258.
37. Morita M, Gravel SP, Chénard V, Sikström K, Zheng L, Alain T, et al. MTORC1 controls mitochondrial activity and biogenesis through 4E-BP-dependent translational regulation. Cell Metab. 2013;18:698–711.
38. Hsieh-Li HM, Chang JG, Jong YJ, Wu MH, Wang NM, Tsai CH, et al. A mouse model for spinal muscular atrophy. Nature genetics [Internet]. 2000;24:66–70. Available from: http://www.nature.com/doifinder/10.1038/71709.
39. 10.1093/hmg/ddq023
Riessland M, Ackermann B, Förster A, Jakubik M, Hauke J, Garbes L, et al. SAHA ameliorates the SMA phenotype in two mouse models for spinal muscular atrophy. Human Molecular Genetics [Internet]. 2010;19:1492–506. Available from: https://academic.oup.com/hmg/article-lookup/doi/10.1093/hmg/ddq023.

40. Morita M, Gravel S-P, Chénard V, Sikström K, Zheng L, Alain T, et al. mTORC1 Controls Mitochondrial Activity and Biogenesis through 4E-BP-Dependent Translational Regulation. Cell Metabolism [Internet]. 2013;18:698–711. Available from: https://linkinghub.elsevier.com/retrieve/pii/S1550413113004130.
41. Schmidt EK, Clavarino G, Ceppi M, Pierre P. SUnSET, a nonradioactive method to monitor protein synthesis. Nature Methods [Internet]. 2009;6:275–7. Available from: http://www.nature.com/articles/nmeth.1314.
42. 10.1242/jcs.214346
Argüello RJ, Reverendo M, Mendes A, Camosseto V, Torres AG, Ribas de Pouplana L, et al. SunRiSE – measuring translation elongation at single-cell resolution by means of flow cytometry. Journal of Cell Science [Internet]. 2018;131:jcs214346. Available from: http://jcs.biologists.org/lookup/doi/10.1242/jcs.214346.
43. RStudio Team. RStudio: Integrated Development Environment for R [Internet]
RStudio Team. RStudio: Integrated Development Environment for R [Internet]. Boston MA. 2019. Available from: http://www.rstudio.com/.
44. Díaz-García CM, Mongeon R, Lahmann C, Koveal D, Zucker H, Yellen G. Neuronal Stimulation Triggers Neuronal Glycolysis and Not Lactate Uptake. Cell Metabolism [Internet]. 2017;26:361–374.e4. Available from: https://www.youtube.com/watch?v=9N3ZmTRfTn0.
45. Klöppel C, Michels C, Zimmer J, Herrmann JM, Riemer J. In yeast redistribution of Sod1 to the mitochondrial intermembrane space provides protection against respiration derived oxidative stress. Biochemical and Biophysical Research Communications [Internet]. 2010;403:114–9. Available from: https://linkinghub.elsevier.com/retrieve/pii/S0006291X10020279.
46. 10.1089/ars.2009.2887
Suzuki YJ, Carini M, Butterfield DA. Protein Carbonylation. Antioxidants & Redox Signaling [Internet]. 2010;12:323–5. Available from: http://www.liebertpub.com/doi/10.1089/ars.2009.2887.
47. Nyström T. Role of oxidative carbonylation in protein quality control and senescence. EMBO J. 2005;24:1311–7.
48. Desagher S, Glowinski J, Prémont J. Pyruvate protects neurons against hydrogen peroxide-induced toxicity. J Neurosci. 1997;17:9060–7.
49. 10.1073/pnas.70.7.1968
Adams MJ, Buehner M, Chandrasekhar K, Ford GC, Hackert ML, Liljas A, et al. Structure-Function Relationships in Lactate Dehydrogenase. Proceedings of the National Academy of Sciences [Internet]. 1973;70:1968–72. Available from: http://www.pnas.org/cgi/doi/10.1073/pnas.70.7.1968.
50. http://doi.wiley.com/10.1002/bio.2879
Kładna A, Marchlewicz M, Piechowska T, Kruk I, Aboul-Enein HY. Reactivity of pyruvic acid and its derivatives towards reactive oxygen species. Luminescence [Internet]. 2015;30:1153–8. Available from: http://doi.wiley.com/10.1002/bio.2879.
51. 10.1074/jbc.M506096200

Sarbassov DD, Sabatini DM. Redox Regulation of the Nutrient-sensitive Raptor-mTOR Pathway and Complex. Journal of Biological Chemistry [Internet]. 2005;280:39505–9. Available from: http://www.jbc.org/lookup/doi/10.1074/jbc.M506096200.

52. 10.1016/j.neuron.2016.12.020
Ashrafi G, Wu Z, Farrell RJ, Ryan TA. GLUT4 Mobilization Supports Energetic Demands of Active Synapses. Neuron [Internet]. Elsevier; 2017;93:606–615.e3. Available from: http://dx.doi.org/10.1016/j.neuron.2016.12.020.

53. 10.1016/j.jalz.2017.09.011
An Y, Varma VR, Varma S, Casanova R, Dammer E, Pletnikova O, et al. Evidence for brain glucose dysregulation in Alzheimer's disease. Alzheimer's & Dementia [Internet]. 2018;14:318–29. Available from: http://doi.wiley.com/10.1016/j.jalz.2017.09.011.

54. Ludolph AC, Langen KJ, Regard M, Herzog H, Kemper B, Kuwert T, et al. Frontal lobe function in amyotrophic lateral sclerosis: a neuropsychologic and positron emission tomography study. Acta Neurologica Scandinavica [Internet]. 1992;85:81–9. Available from: http://www.ncbi.nlm.nih.gov/pubmed/1574993.

55. 10.1101/517649v1
Manzo E, Lorenzini I, Barrameda D, O'Conner AG, Barrows JM, Starr A, et al. Glycolysis upregulation is neuroprotective as a compensatory mechanism in ALS. bioRxiv [Internet]. 2019;517649. Available from: https://www.biorxiv.org/content/10.1101/517649v1.

56. Wang H, Guo W, Mitra J, Hegde PM, Vandoorne T, Eckelmann BJ, et al. Mutant FUS causes DNA ligation defects to inhibit oxidative damage repair in Amyotrophic Lateral Sclerosis. Nature Communications [Internet]. Nature Publishing Group; 2018;9:3683. Available from: http://www.nature.com/articles/s41467-018-06111-6.

57. Hung CH-L, Cheng SS-Y, Cheung Y-T, Wuwongse S, Zhang NQ, Ho Y-S, et al. A reciprocal relationship between reactive oxygen species and mitochondrial dynamics in neurodegeneration. Redox Biology [Internet]. Elsevier B.V.; 2018;14:7–19. Available from: https://linkinghub.elsevier.com/retrieve/pii/S2213231717305037.

58. Robak J, Marcinkiewicz E. Scavenging of reactive oxygen species as the mechanism of drug action. Polish journal of pharmacology [Internet]. 1995 [cited 2020 Jun 14];47:89–98. Available from: http://www.ncbi.nlm.nih.gov/pubmed/8688896.

59. Perez-Riverol Y, Csordas A, Bai J, Bernal-Llinares M, Hewapathirana S, Kundu DJ, et al. The PRIDE database and related tools and resources in 2019: improving support for quantification data. Nucleic Acids Research [Internet]. 2019;47:D442–50. Available from: http://www.ncbi.nlm.nih.gov/pubmed/30395289.

Figures

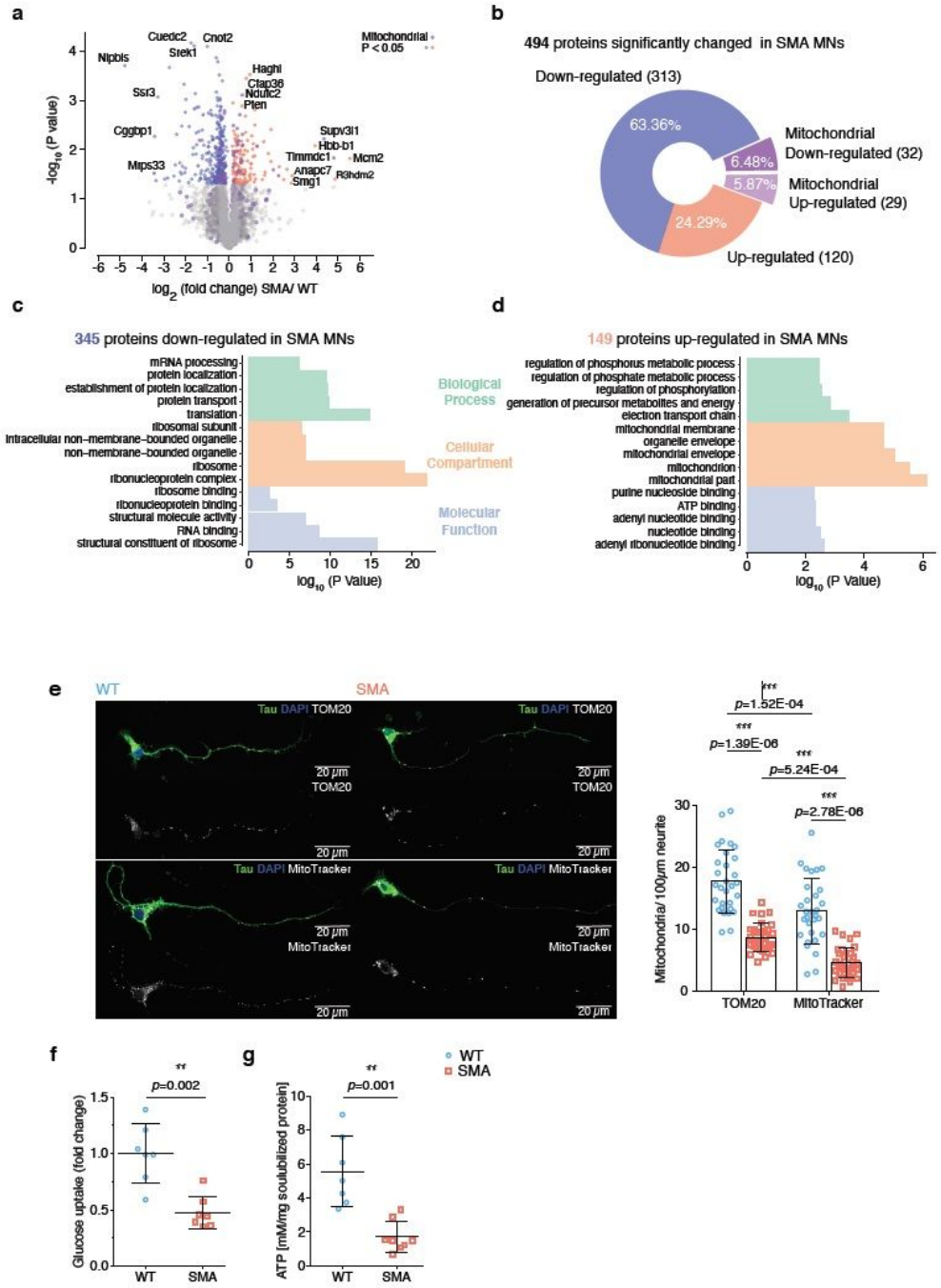

Figure 1

Defectivemitochondria result in reduced ATP levels in SMA motoneurons (MNs). a, b Volcano plot (a) andpie chart (b) of whole proteome analysis comparing WT and SMA MNs; plotted p-values (-log10) against fold changes (log2, SMA/ WT). Four independent samples of WT MNs and three independent samples of SMA MNs were used for analysis. P-values were determined using unpaired two-sided t-test. Proteins with p < 0.05 are highlighted in blue (313 down-regulated) and red (120 up-regulated), and

proteins with localization in mitochondria are marked in purple (32 down-regulated and 29 up-regulated). c, d Gene ontology (GO) analysis of 345 down-regulated (c) and 149 up-regulated proteins (d) in SMA MNs. The 5 most significant terms of each category are shown. e Representative images and quantification of mitochondria in 100 □m long primary axons of WT and SMA MNs labelled with anti-Tau antibody (green), DAPI (blue) and anti-TOM20 antibody or MitoTracker® (white). Scale bars: 20 μm. Each dot represents the average number of mitochondria in each neuron (n=30; biological replicates N=3). Two-way ANOVA with Tukey HSD post hoc analysis was used to determine statistical significance for multiple comparisons. Bar graphs depict the mean ± s.d. ***p <0.001. f Glucose uptake in WT and SMA MNs. Each dot represents data from biological replicates (N=7). g ATP levels in WT (N=7)and SMA MNs(N=8). Each dot represents data from biological replicates. f,g Two-tailed unpaired t-test was used to determine statistical significance. Bar graphs depict the mean ± s.d. **p <0.01, ***p <0.001. Blue circles represent WT MNs and red squares represent SMA MNs. 10DIV MNs were used.

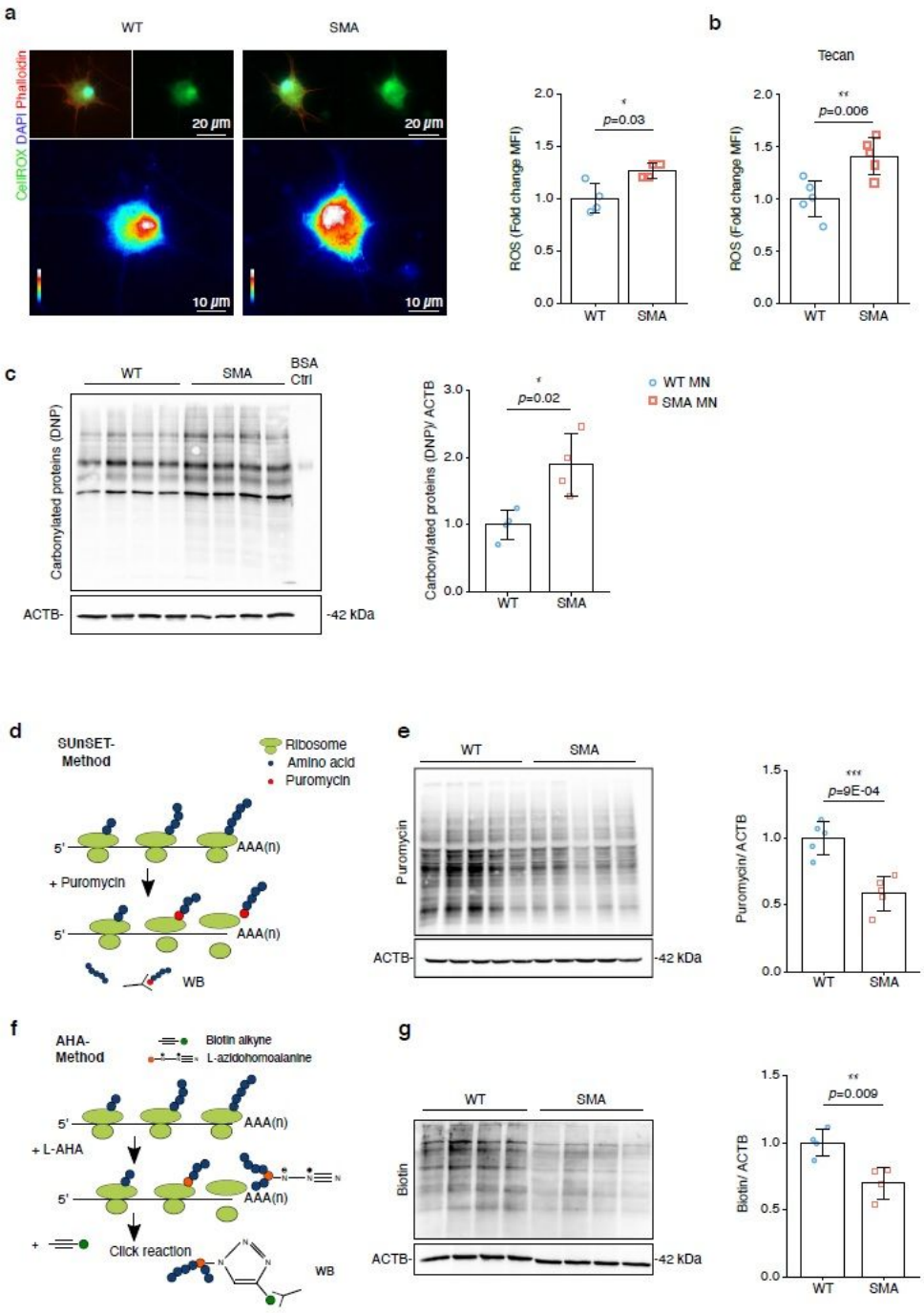

Figure 2

ROS levels are elevated, proteins are hyper-carbonylated and protein synthesis is impaired in SMA MNs. a Representative images and quantification of WT and SMA MNs labelled with CellROX® (green and rainbow color) for reactive oxygen species (ROS) detection, DAPI (blue) and Phalloidine (red). Rainbow color indicates the intensity of CellROX® signal. Scale bar of enlarged CellROX® images: 10 µm; Scale bar of neuron: 20 µm. Quantification of mean fluorescence intensity of the CellROX® signal in WT and

SMA MN (red squares) (n=40, N=4). b Quantification of CellROX® signal of WT and SMA MNs measured with microplate reader (N=5). c Western blot analysis and quantification of carbonylated proteins (DNP = 2,4-dinitrophenyl) in 10DIV WT and SMA MNs (N=4). Quantification of DNP signal was normalized to ACTB. d Schematic drawing of SUnSET method. Puromycin labels newly synthesized proteins. Puromycin is detected by anti-puromycin antibody. eSunSET assay in WT and SMA MNs (N=5). ACTB was used as loading control. f Schematic drawing of the AHA method. L-azidohomoalanine (L-AHA) is incorporated into newly synthesized proteins, followed by click chemistry reaction with biotin alkyne. Biotin labelled proteins can be detected by western blot analysis. g AHA assay in WT and SMA MNs (N=4). ACTB was used as loading control. Blue circles represent data from WT and red squares represent SMA MNs. All bar graphs depict the mean ± s.d. Two-tailed unpaired t-test was used on independent biological replicates to determine statistical significance *p <0.05, **p <0.01, ***p <0.001.

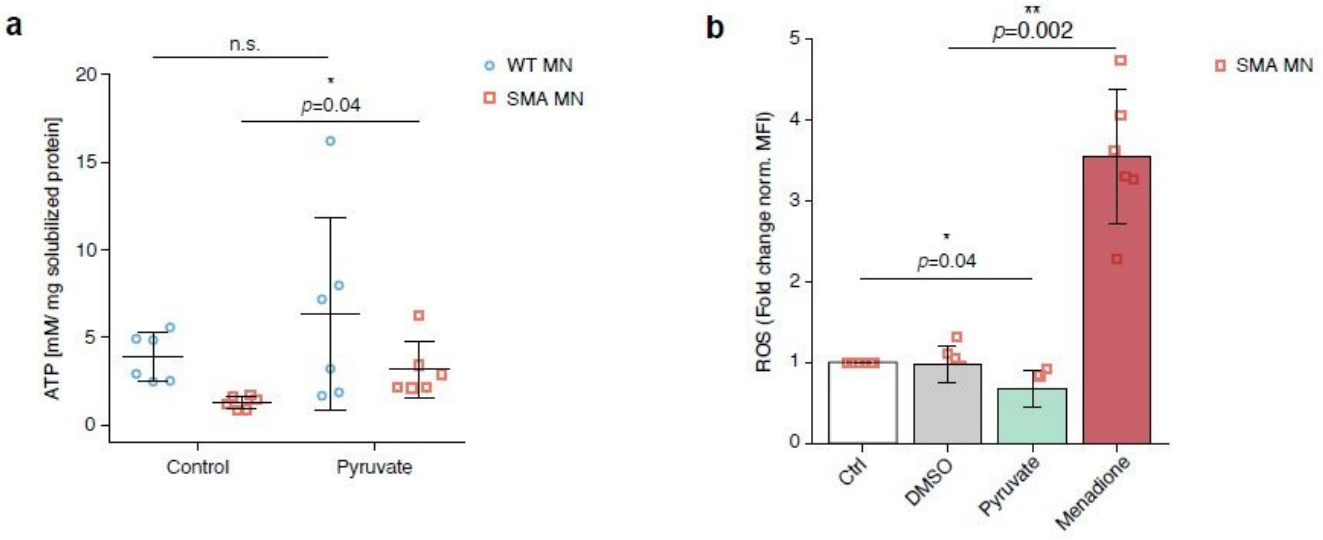

Figure 3

Pyruvate restores ATP levels and reduces ROS levels in SMA MNs a ATP levels in WT and SMA MNs normalized to solubilized protein. Two-tailed unpaired t-test was used on independent biological replicates to determine statistical significance *p <0.05. b ROS levels of SMA MNs. Two-tailed unpaired t-tests with Holm-Bonferroni correction for multiple comparisons were used to determine statistical significance. **p <0.01 Blue circles represent data from WT and red squares represent SMA MNs. Each dot represents the quantification of individual biological replicates (N=6).

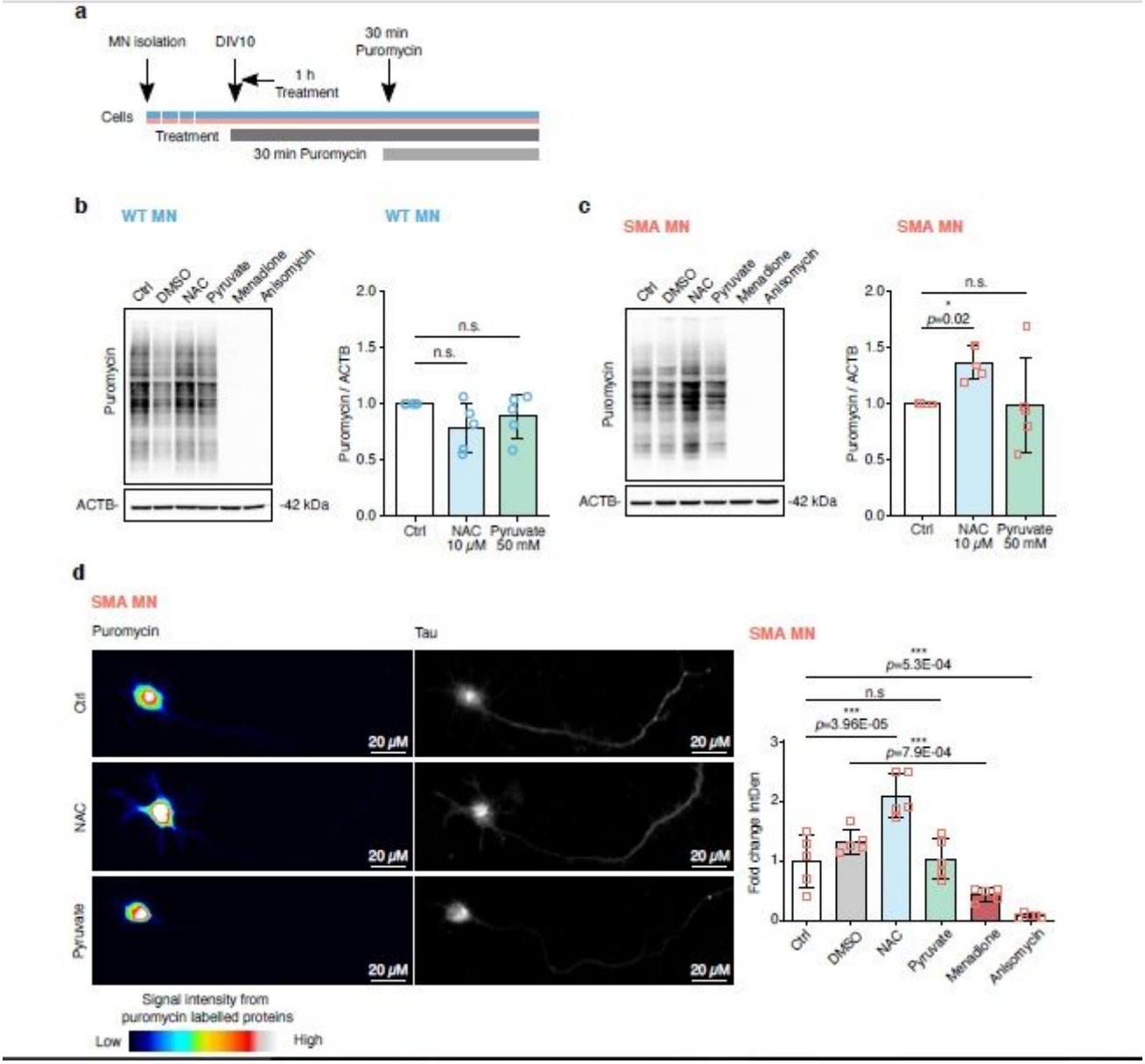

Figure 4

Anti-oxidant NAC restores protein synthesis in SMA MNs a Scheme of experimental design. 10DIV MNs were treated with 10 μM NAC or 50 mM pyruvate for 1 h. Cells were incubated with 1 μM puromycin for 30 min before analysis. bSUnSET assay after ROS modification in WT MNs (N=5). cSUnSET assay after ROS modification in SMA MNs (N=5). b,c Two-tailed unpaired t-tests with Holm-Bonferroni correction for multiple comparisons were used to determine statistical significance. n.s. p >0.05, **p <0.01. d Representative images of neurons after SUnSET assay after ROS modification in SMA MNs. TAU staining shows whole neuronal morphology and puromycin signal represents protein synthesis in given time. Rainbow color scale showed the intensity of puromycin. Scale bar: 20 μm. 10 μM NAC enhanced and 100 μM menadione or 50 μM anisomycin inhibited protein synthesis in SMA MNs. Each dot represents the average intensity of 15 neurons (N=5). One-way ANOVA with Tukey HSD post hoc analysis was used to determine statistical significance for multiple comparisons. Bar graphs depict the mean ± s.d.n.s. p >0.05, ***p <0.001.

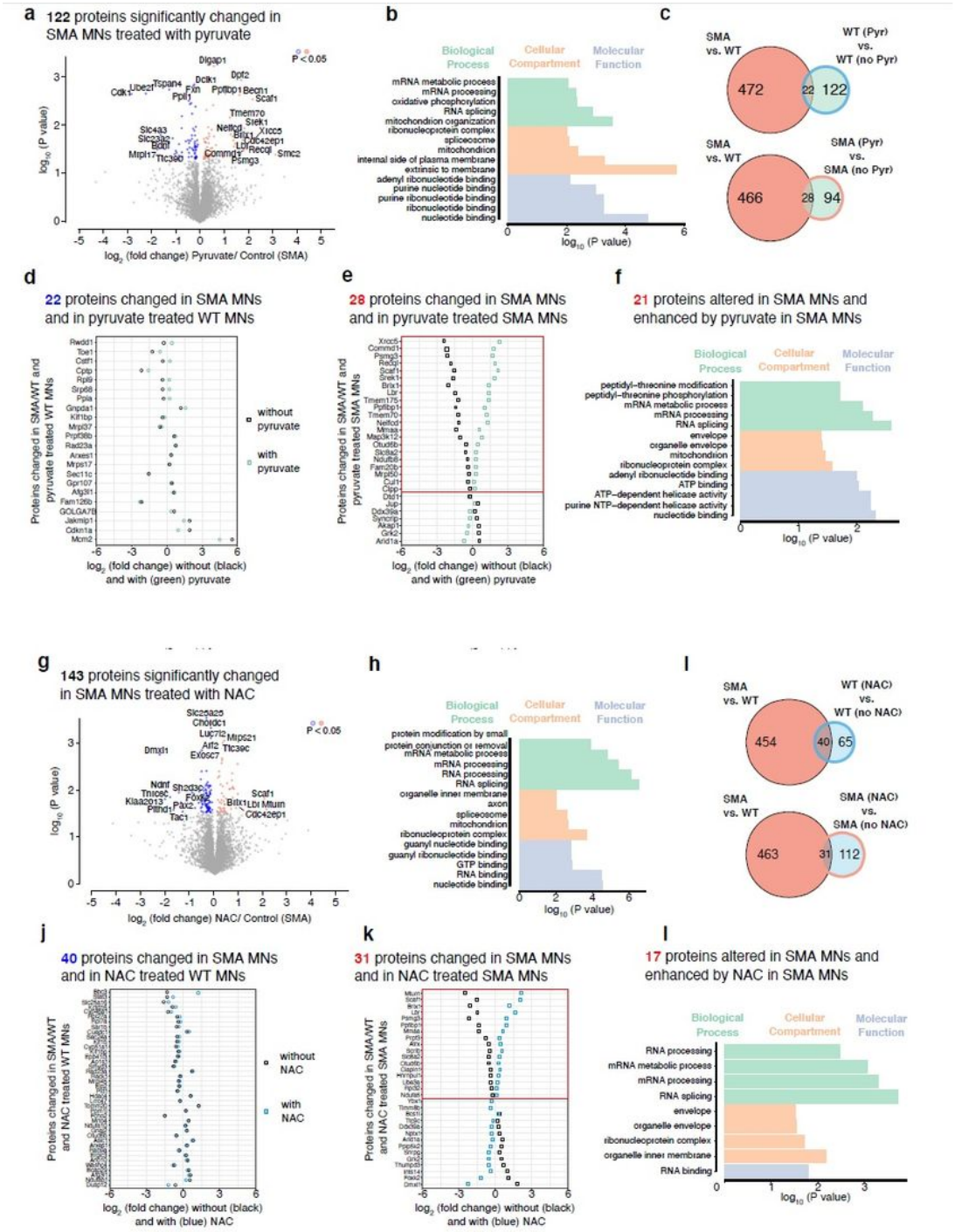

Figure 5

NAC and pyruvate modify proteome in SMA MNs with a minor impact on WT MNs a Volcano plot of whole proteome analysis in SMA MNs after pyruvate treatment; plotted p-value (-log10) against fold change (log2). (N=3). P-values were determined using an unpaired two-sided t-test. Significantly changed proteins with p < 0.05 are highlighted in blue (down-regulated)/ red (up-regulated). b GO term analysis of 112 significantly changed proteins by pyruvate treatment in SMA MNs. c Venn diagram showing overlap

of significantly altered proteins in SMA compared to WT and significantly changed proteins by pyruvate in WT MNs or in SMA MNs. d Representing 22 proteins changed in SMA MNs compared to WT MNs, and pyruvate treated WT MNs compared to non-treated WT MNs; plotted fold change (log2) comparing with and without pyruvate treatment. e Representing 28 proteins changed in SMA MNs compared to WT MNs, and pyruvate treated SMA MNs compared to non-treated SMA MNs; plotted fold change (log2) comparing with and without pyruvate treatment. f GO term analysis of 21 proteins changed in SMA MNs compared to WT MNs and significantly up-regulated by pyruvate treatment in SMA MNs. g Volcano plot of whole proteome analysis comparing NAC treated and non-treated SMA MNs; plotted p-value (-log10) against fold change (log2). (n=3). P-values were determined using an unpaired two-sided t-test. Significantly changed proteins with $p < 0.05$ are highlighted in blue (down-regulated)/ red (up-regulated). h GO term analysis of 142 significantly changed proteins by NAC treatment in SMA MNs. iVenn diagram showing overlap of significantly altered proteins in SMA compared to WT and significantly changed proteins by NAC in WT MNs or in SMA MNs. j 40 proteins changed in SMA MNs compared to WT MNs, and NAC treatment in WT MNs; plotted fold change (log2) with and without NAC treatment k 31 proteins changed in SMA MNs compared to WT MNs, and NAC treatment in SMA MNs; plotted fold change (log2) with and without NAC treatment. l GO term analysis of 17 proteins changed in SMA MNs compared to WT MNs, and significantly increased by NAC treatment in SMA MNs.

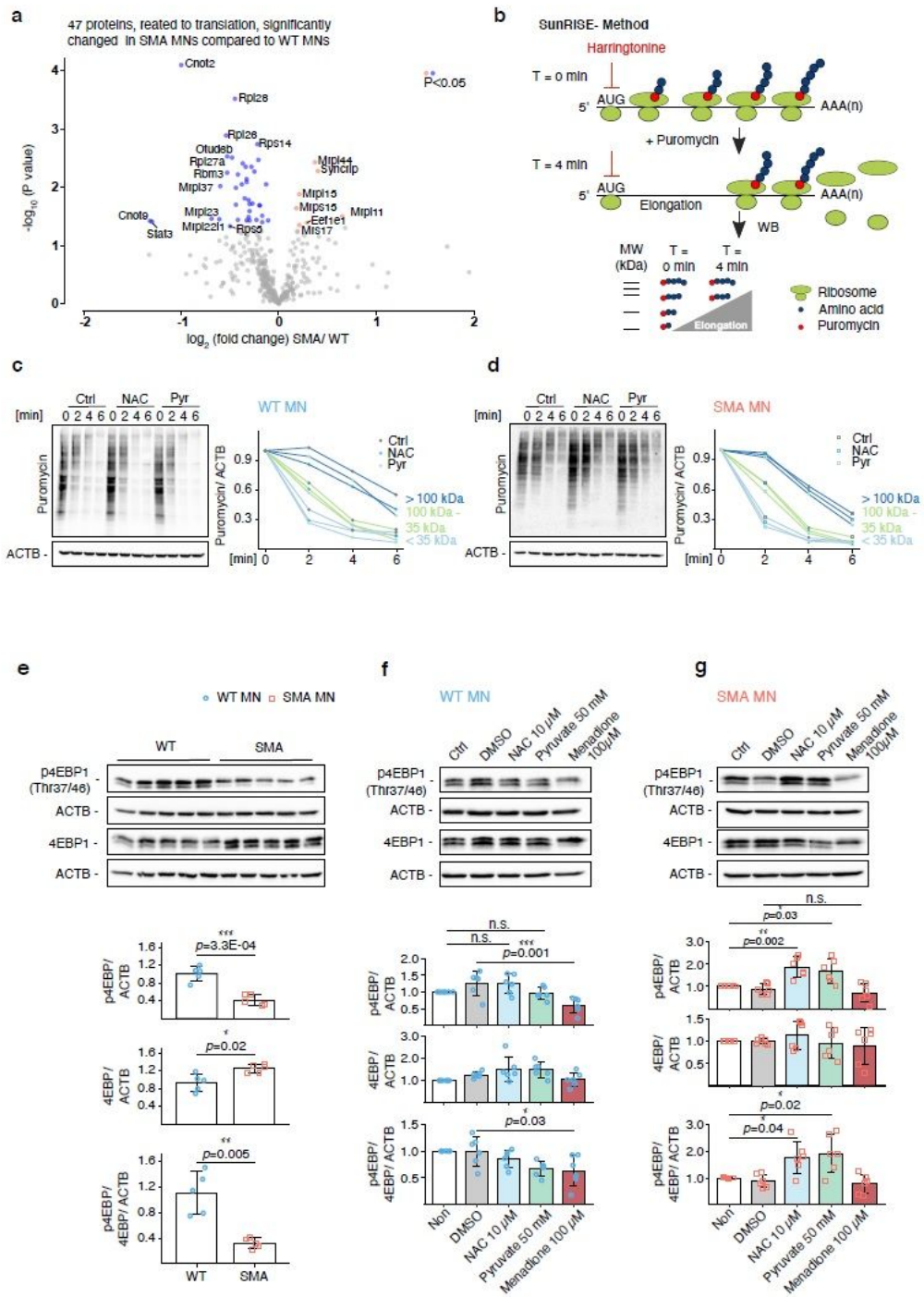

Figure 6

ROS regulates initiation of protein translation without changing translation elongation a Volcano plot of translation related proteins comparing WT and SMA MNs; plotted p-value (-log10) against fold change (log2, SMA/ WT). Four independent samples of WT MNs and three independent samples for SMA MNs were used for analysis. P-values were determined using an unpaired two-sided t-test. Proteins with p < 0.05 are highlighted in blue (down-regulated) and red (up-regulated). b Scheme of SunRiSE assay.

Translation initiation of 10DIV WT or SMA MNs was blocked with 2 µg/ml harringtonine at different time-points before adding 10 µg/ml puromycin for 10 min. c, d NAC or pyruvate does not change elongation speed in WT (c)or SMA (d) MNs. e Western blot analysis measuringtranslation initiation with p-4EBP1 levels in WT (blue circles) and SMA MNs (red squares) (N=5). Measured by phosphosite-specific p-4EBP1 and total 4EBP1 antibodies. ATCB was used as loading control. Each dot represents the data from individual biological replicates. Two-tailed unpaired t-test was used to determine statistical significance *p <0.05, **p <0.01, ***p <0.001. f, g Western blot analysis shows that pharmacologically modifying ROS levels changes p-4EBP1 levelsin WT MNs (N=6) (f) and SMA MNs (N=6) (g). Each dot represents the data from individual biological replicates. One-way ANOVA with Tukey HSD post hoc analysis was used to determine statistical significance for multiple comparisons. Bar graphs depict the mean ± s.d.n.s. p >0.05, *p <0.05, **p <0.01, ***p <0.001.

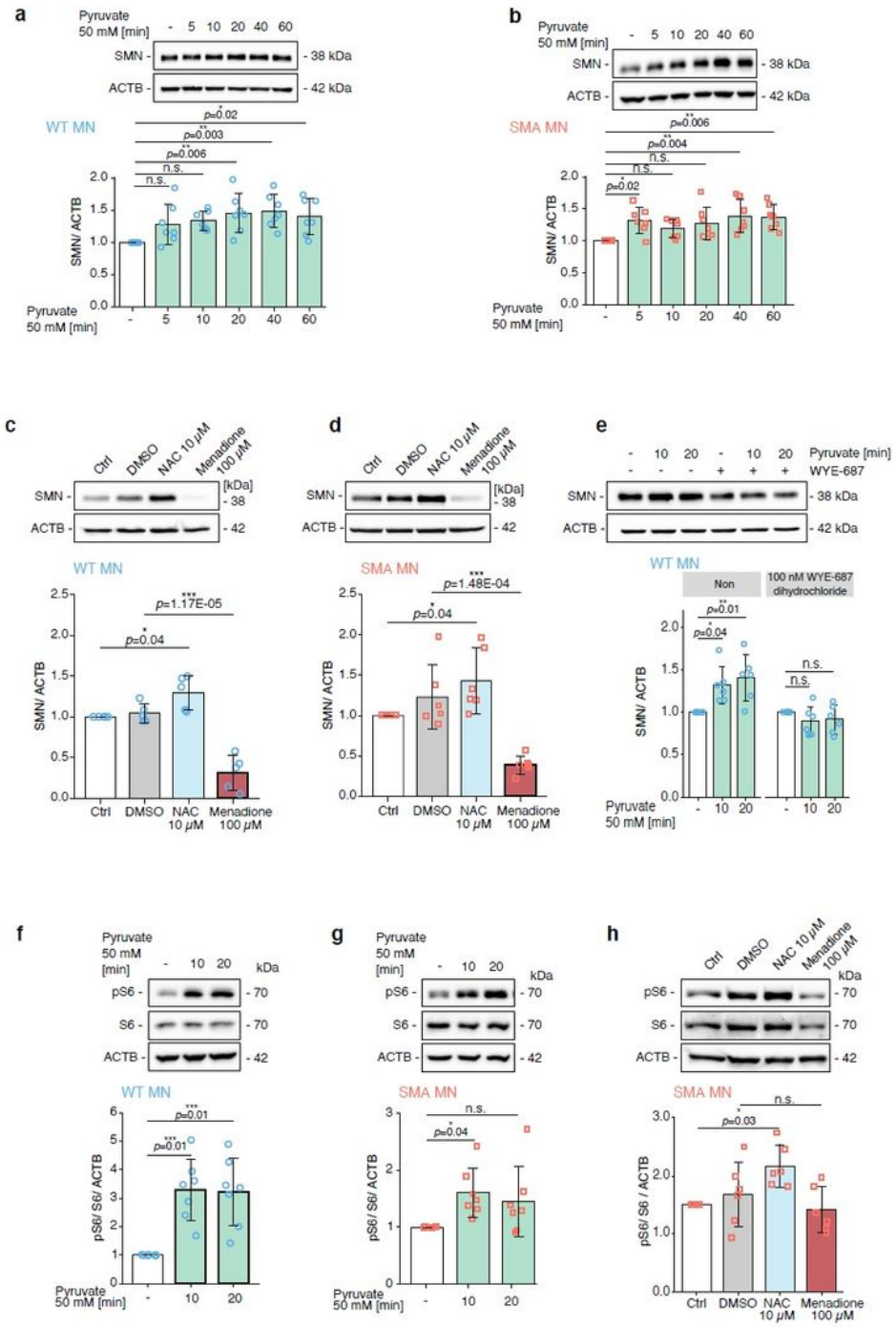

Figure 7

SMN protein levels are regulated mTOR-dependently by pyruvate and ROS modifying drugs. a-d Representative western blot images and quantification of SMN levels after 1h pyruvate (a, b) and ROS modulating drugs (c, d) treatment in WT MNs (a, c) and SMA MNs (b, d). e Treatment of 100 nM WYE-687 dihydrochloride blocks mTOR dependent increase of SMN levels after pyruvate treatment in WT MNs. f-h Representative western blot and quantification of phosphorylated S6 and total S6 protein levelsafter

pyruvate treatment in WT MNs (f, N=7) and in SMA MNs (g, N=7) and ROS modulating drugs in SMA MNs(N=4) (h). a,bOne-way ANOVA with Dunnett post hoc analysis was used to compare each timepoint with the control. Each dot represents the quantification of individual biological replicates. Bar graphs depict the mean ± s.d.n.s. p >0.05, *p <0.05, **p <0.01. c-h One-way ANOVA with Tukey HSD post hoc analysis was used to determine statistical significance for multiple comparisons. Each dot represents the quantification of individual biological replicates. Bar graphs depict the mean ± s.d.n.s. p >0.05, *p <0.05, **p <0.01, ***p <0.001.

Supplementary Files

This is a list of supplementary files associated with this preprint. Click to download.

- Additionalfile3MSSourcedata.xlsx
- Additionalfile2Supplementarytables.docx
- Additionalfile1Supplementaryfigures.pdf